International Journal of Solids and Structures 225 (2021) 111048

Contents lists available at ScienceDirect

International Journal of Solids and Structures

journal homepage: www.elsevier.com/locate/ijsolstr

Anisotropic damage model for concrete and other quasi-brittle materials

Jani Vilppo [a], Reijo Kouhia [a,*], Juha Hartikainen [a], Kari Kolari [b], Alexis Fedoroff [b], Kim Calonius [b]

[a] Tampere University, Civil Engineering, P.O. Box 600, FI-33101 Tampere, Finland
[b] VTT Technical Research Center of Finland, P.O. Box 1000, FI-02044 VTT Espoo, Finland

ARTICLE INFO

Article history:
Received 2 January 2021
Received in revised form 4 March 2021
Accepted 30 March 2021

Keywords:
Anisotropic damage
Axial splitting
Elastic-brittle material
Concrete
Ottosen's 4-parameter criterion
Constitutive equations
The specific Gibbs free energy
Dissipation potential
Failure modes

ABSTRACT

A thermodynamically consistent formulation to model anisotropic damage for quasi-brittle materials is proposed. The model is based on proper expressions for the specific Gibbs free energy and the complementary form of the dissipation potential. Damaging of the material is described by a symmetric positive definite second order damage tensor. Especially, the failure surface is formulated in such a way that it will mimic the behaviour of the well known Ottosen's four parameter failure surface. While testing the model against the experimental results found in literature, the results were in good agreement in uniaxial tensile and compressive loadings as well as in biaxial compression. Besides the correct failure stress states, the model predicts the correct failure modes of concrete: axial splitting along the direction of uniaxial compression and tensile damaging normal to the direction of tension.

1. Introduction

Cementitious materials, like concrete, rocks and some ceramics can show considerable ductility under certain stress states, while being extremely brittle under purely tensile loadings. Being one of the most commonly used construction materials, concrete has been subjected to a significant amount of research including failure behaviour in consideration of different loading conditions and micro-structural defects such as voids, inhomogeneities and micro-cracks. Particular characteristics of the failure behaviour include gradual loss of the elasticity, volume dilatancy and strain softening, which are consequences of the propagation and coalescence of micro-cracks leading ultimately to the material failure (van Mier, 1986; Dragon et al., 2000). It is well-known that brittle materials like concrete and rock fail by axial-splitting along the direction of uniaxial compression. Although the micromechanics of axial-splitting have been studied quite extensively e.g. Adams and Sines (1978), Brace and Bombolakis (1963), Horii and Nemat-Nasser (1982), Kendall (1978), very little attention has been paid on the correct failure modes in the development of continuum models. As discussed by Schreyer (2007) the classical stress criteria do not have the flexibility to reflect the failure modes for various of stress states and "none predicts axial splitting". In the authors' knowledge only few continuum models can predict the compressive axial-splitting, e.g. Basista (2003), Halm et al. (2003), Kolari (2007), Murakami and Kamiya (1997), Schreyer (2007), Yazdani and Schreyer (1988), Yaghoubi et al. (2014). Furthermore, the stress–strain behaviour of concrete is highly anisotropic because of the substantial difference between its tensile and compressive strengths.

Several constitutive models based on plasticity theory have been presented to describe the inelastic behaviour of concrete, see e.g. Mikkola and Schnobrich (1970), Willam and Warnke (1975), Dragon and Mróz (1979), Menétrey and Willam (1995), Grassl et al. (2002), Papanikolaou and Kappos (2007). The main drawback of these models is that they fail to represent the gradual loss of elasticity due to damage and micro-cracking.

Damage has been modelled by means of scalar, vectorial or tensorial damage variables. Scalar damage variables that were first introduced by Kachanov (1958) are easy to implement, and hence widely applied, e.g. Lee and Fenves (1998),Grassl and Jirásek (2006), Jason et al. (2006),Nguyen and Korsunsky (2008), and Voyiadjis and Taqieddin (2009). Mazars and Pijaudier-Cabot (1996), considered isotropic damage and presented relationships between damage and fracture mechanics theories. The damage of rock-like materials, however, is definitely anisotropic due to the

* Corresponding author.
E-mail addresses: jani.vilppo@tuni.fi (J. Vilppo), reijo.kouhia@tuni.fi (R. Kouhia), juha.hartikainen@tuni.fi (J. Hartikainen), kari.kolari@vtt.fi (K. Kolari), alexis.fedoroff@vtt.fi (A. Fedoroff), kim.calonius@vtt.fi (K. Calonius).

https://doi.org/10.1016/j.ijsolstr.2021.111048
0020-7683/

orientation of micro-cracks depending on the stress state. This feature can be described only by vectorial or tensorial damage variables. Vectorial damage variables have been used by Davison and Stevens (1973) and Mikkola and Piila (1984). Second-order damage tensors have been utilized by authors such as Murakami and Ohno (1981), Simo and Ju (1987), Yazdani and Schreyer (1990), Lubarda et al. (1994), Murakami and Kamiya (1997), Dragon et al. (2000), Badel et al. (2007) and Murakami (2012). In addition, Ortiz (1985) has used a fourth-order compliance tensor in a two-phase continuum damage model to represent the damage process of concrete. Higher-order tensor description for damage has also been discussed in Ju (1990), Chaboche (1993), Cauvin and Testa (1999), Olsen-Kettle (2018), Olsen-Kettle (2018).

Several authors have combined plasticity and damage to model the failure of concrete. For example, Grassl and Jirásek (2006), Cicekli et al. (2007), Jefferson (2003), Jefferson et al. (2016), and Voyiadjis et al. (2008) have proposed a mixed plasticity anisotropic damage model for concrete using scalar and tensorial damage variables. The combination of plasticity and anisotropic damage can easily lead to complex models, see e.g. Yazdani and Schreyer (1990) and Ibrahimbegović et al. (2003). On the other hand, since the inelastic behaviour of concrete is rather due to damage and micro-cracking than plastic deformations, as presented by Mazars and Pijaudier-Cabot (1989) and Mazars and Pijaudier-Cabot (1996), models based merely on damage and micro-cracking have been formulated regularly. Although these models are not capable of capturing features of rock-like materials such as irreversible deformations during loading like inelastic volume expansion in compression (Mazars (1984)), they are less complicated to implement and thereby more popular than the coupled plastic-damage models.

The special feature of brittle materials is that they behave significantly differently in tension and compression which requires a proper description of a failure criterion. Among several failure criteria for concrete, the three parameter Mohr-Couloumb criterion with a tension cut-off is widely used. As for antecedent failure criteria, those by Willam and Warnke (1975) and Bresler and Pister (1958), as well as the four parameter criteria by Ottosen (1977) and Hsieh et al. (1979) can be mentioned. The microplane approach, originally proposed by Baant and Oh (1985), has recently got much attention, see e.g. Bažant et al. (2000), Valentini and Hofstetter (2013).

Lubliner et al. (1989) proposed a continuum damage model, the well-known Barcelona model, using a scalar damage variable for the degradation of both the volumetric and distortional elasticity, separately. Lee (1996) and Lee and Fenves (1998) revised the Barcelona model by using two independent scalar damage variables to represent properly the cyclic behaviour of concrete. Their model has been implemented in the commercial finite element software Abaqus by Dassault Systémes (2020). A similar approach is carried out by Grassl et al. (2013), and a selection of 3D concrete models is reviewed by Valentini and Hofstetter (2013).

Fracture energy based approach to model inelastic behaviour of concrete is proposed by Etse and Willam (1994) and a similar fracture mechanics approach utilizing the Menétrey-Willam failure surface is given by Červenka and Papanikolaou (2008). Furthermore, a discrete crack approach is formulated by Gálvez et al. (2002).

Classical elasto-plastic theory for tri-axial modelling of plain concrete and numerical implementations are presented in Lu et al. (2016), Lu et al. (2019), Lu et al. (2020).

A recent review of concrete model and numerical implementations is presented by Oliveira et al. (2020). The smeared crack approach, which is one of the most used in numerical analysis of concrete structures is analysed by Rimkus et al. (2020).

One of the most successful failure criteria is the Ottosen model (Ottosen, 1977). It captures the relevant features of concrete failure under various multiaxial stress states. A combined elastic–plastic damaging approach based on Ottosen's criterion, with two scalar damage variables, is given by Contrafatto and Cuomo (2003). It is based on their general formulation presented in Contrafatto and Cuomo (2002), see also Contrafatto and Cuomo (2006), Contrafatto and Cuomo (2007). In a recent study by Zhang et al. (2020), the Ottosen model is formulated as an elasto-plastic model with a non-associated flow rule. It is also amended by a cap model to describe the yielding behaviour under high hydrostatic pressure.

In the present study, a model for quasi-brittle materials, like concrete is proposed with the following main objectives:

1. To be able to capture the basic brittle failure modes: a) axial splitting along the direction of unconfined uniaxial compression, b) damaging perpendicular to the direction of uniaxial unconfined tension.
2. To predict correct failure stresses as described by the failure surface of Ottosen.
3. To obtain a formulation which is thermodynamically consistent.
4. To have parameters which are easily obtained from experiments without using any least-squares or even more sophisticated data fitting procedures.

The structure of the paper is as follows: Section 2 describes the main features and parameters of the Ottosen's four parameter failure criterion.

In Section 3.1, the general thermodynamically consistent formulation in terms of free energy and dissipation potential is described.

Section 3.2 describes the particular choices for the specific Gibbs free energy and dissipation potential. The isotropic potential functions are written in terms of invariants forming a functional, i.e. irreducible basis having two symmetric second-order tensor variables, namely the stress tensor $\boldsymbol{\sigma}$ and the damage tensor $\boldsymbol{D}$, which resembles the crack density tensor of Kachanov (1992). Thus, the eigenvalues of $\boldsymbol{D}$ are not limited to the value of 1. The evolution of damage is described in terms of the strain tensor $\boldsymbol{\varepsilon}$, stress and the thermodynamic conjugate force $\boldsymbol{Y}$ for damage rate. The eigenvalues of the strain tensor are applied in the evolution equation to describe the physically correct failure modes both in compression and tension.

In Section 3.3, the determination of material parameters is described in detail.

Section 4 is devoted into numerical verification of the model. Besides the unconfined uniaxial compression and tension, the biaxial and equibiaxial compression are considered. The results are compared with the well-known experimental results of Kupfer et al. (1969).

2. Ottosen's four parameter criterion

In 1977, Ottosen proposed a failure surface in terms of three stress invariants for short-term loading of concrete capturing the relevant failure stress states of brittle materials (Ottosen, 1977; Ottosen, 1980; Ottosen and Ristinmaa, 2005). The failure surface has a curved shape on the meridian plane. On the deviatoric plane, the shape evolves from triangular to more circular form along with increasing hydrostatic pressure. In addition, the failure surface deals with the feature that concrete behaves significantly differently in tension and compression. The criterion agrees well with the experimental results for different stress states such as triaxial stresses.

The Ottosen's 4-parameter failure criterion has the form

$$f(I_1, J_2, \cos 3\theta) = A\frac{J_2}{\sigma_c} + \Lambda(\theta)\sqrt{J_2} + BI_1 - \sigma_c = 0, \tag{1}$$

where $I_1 = \mathrm{tr}\boldsymbol{\sigma}$is the first invariant of the stress tensor $\boldsymbol{\sigma}$, and $J_2 = \frac{1}{2}\mathrm{tr}\boldsymbol{s}^2$ the second invariant of the deviatoric stress tensor $\boldsymbol{s} = \boldsymbol{\sigma} - \sigma_m\boldsymbol{I}$. Furthermore, A and B are non-negative dimensionless material parameters, σ_c stands for the uniaxial compressive strength of the material, and σ_m is the mean normal stress $\sigma_m = \frac{1}{3}I_1$.

The function $\Lambda = \Lambda(\theta)$ in defined as

$$\Lambda(\theta) = \begin{cases} k_1 \cos[\frac{1}{3}\arccos(k_2 \cos 3\theta)] & \text{if} \quad \cos 3\theta \geqslant 0 \\ k_1 \cos[\frac{1}{3}\pi - \frac{1}{3}\arccos(-k_2 \cos 3\theta)] & \text{if} \quad \cos 3\theta \leq 0 \end{cases}, \tag{2}$$

where θ is the Lode angle. The size factor k_1 and the shape factor k_2 are dimensionless material parameters such that

$$k_1 \geqslant 0, \quad 0 \leqslant k_2 \leq 1. \tag{3}$$

The Lode angle is defined on the deviatoric plane in terms of the deviatoric invariants as

$$\theta = \frac{1}{3}\arccos\left(\frac{3\sqrt{3}}{2}\frac{J_3}{J_2^{3/2}}\right), \tag{4}$$

where $J_3 = \det \boldsymbol{s}$ is the third invariant of the deviatoric stress tensor.

The four dimensionless non-negative parameters A, B, k_1 and k_2 can be determined from experiments by using e.g. the following four failure stress states (Ottosen and Ristinmaa, 2005):

(i) uniaxial compressive strength σ_c,
(ii) uniaxial tensile strength σ_t,
(iii) equibiaxial compressive strength σ_{bc},
(iv) and an arbitrary failure state on the compressive meridian: $(I_1, \sqrt{J_2}) = (\xi_1\sigma_c, \xi_2\sigma_c)$.

States (i) and (iv) lie on the compressive meridian ($\theta = \pi/3$) and states (ii) and (iii) on the tensile meridian ($\theta = 0$). Substituting the four failure stress states points into criterion (1) and solving the resulting equations for A, B, k_1 and k_2 leads to the expressions

$$A = -\frac{1}{\xi_2}\left(\zeta B + \sqrt{3}\right), \tag{5}$$

$$B = \frac{\frac{3\sigma_c^2}{\sigma_{bc}\sigma_t}\xi_2 - \sqrt{3}}{\zeta + 9\frac{\sigma_c}{\sigma_{bc}-\sigma_t}\xi_2}, \tag{6}$$

$$k_1 = \frac{2}{\sqrt{3}}\sqrt{\Lambda_t^2 + \Lambda_c^2 - \Lambda_t\Lambda_c}, \tag{7}$$

$$k_2 = 4\left(\frac{\Lambda_t}{k_1}\right)^3 - 3\frac{\Lambda_t}{k_1}, \tag{8}$$

where

$$\zeta = \frac{\sqrt{3}\xi_1 + 3\xi_2}{\sqrt{3}\xi_2 - 1}, \tag{9}$$

$$\Lambda_t = \Lambda(0) = \sqrt{3}\left(\frac{\sigma_c}{\sigma_{bc}} + 2B - \frac{\sigma_{bc}}{3\sigma_c}A\right), \tag{10}$$

$$\Lambda_c = \Lambda(\pi/3) = \sqrt{3}\left(1 + B - \frac{1}{3}A\right). \tag{11}$$

Figs. 1 and 2 illustrate the Ottosen failure criterion. For comparison, figures also show graphs of the tension cut-off Mohr–Coulomb failure criterion for the friction angle of $\phi \approx 37^\circ$ being in accordance with the experimental results (Dahl, 1992), and graphs of the Barcelona failure criterion (Lubliner et al., 1989) which is represented for the equal characteristics of the failure states (i)–(iii) next. The parameters are taken from Ottosen (1977) which are based on the experimental results by Kupfer et al. (1969), Balmer (1949) and Richart et al. (1928): $\sigma_t/\sigma_c = 0.1, \sigma_{bc}/\sigma_c = 1.16$ and $\xi_1 = -5\sqrt{3}, \xi_2 = 4/\sqrt{2}$, resulting in values

$$A = 1.276, \quad B = 3.196, \quad k_1 = 11.74, \quad k_2 = 0.9801. \tag{12}$$

In the pdf the equation (12) is splitted in a strange way. Here it looks fine in a one line form.

3. Present constitutive model

The objective of the present study is to propose a model that predicts both the correct failure stress states and the correct principal failure modes of elastic-brittle materials. Special attention is paid on the compressive axial splitting and tensile failure modes. The formulation is based on finding proper expressions for the specific Gibbs free energy and dissipation potential, and on the exploitation of the general constitutive relations.

3.1. Thermodynamic formulation

Assuming constant density, i.e. $\rho = \rho_0$, and linear kinematics, the dissipation inequality is presented in terms of the specific Helmholtz free energy ψ, the specific entropy η, the absolute temperature ϑ, the stress tensor, the strain tensor $\boldsymbol{\varepsilon}$ and the heat flow vector $\boldsymbol{q}$ as

$$\gamma = -\rho_0\dot{\psi} - \rho_0\eta\dot{\vartheta} + \mathrm{tr}(\boldsymbol{\sigma}^{\mathrm{T}}\dot{\boldsymbol{\varepsilon}}) - \frac{\mathrm{grad}\vartheta}{\vartheta}\boldsymbol{q} \geqslant 0, \tag{13}$$

where γ is the power of dissipation and the dot signifies the material time derivative. Introducing the specific Gibbs free energy $\psi^c = \psi^c(\vartheta, \boldsymbol{\sigma}, \boldsymbol{D}, \boldsymbol{\kappa})$, where $\boldsymbol{D}$ is the second order damage tensor and $\boldsymbol{\kappa}$denotes a set of internal variables, and using the Legendre transformation

$$\rho_0\psi(\vartheta, \boldsymbol{\varepsilon}, \boldsymbol{D}, \boldsymbol{\kappa}) + \rho_0\psi^c(\vartheta, \boldsymbol{\sigma}, \boldsymbol{D}, \boldsymbol{\kappa}) = \mathrm{tr}(\boldsymbol{\sigma}^{\mathrm{T}}\boldsymbol{\varepsilon}), \tag{14}$$

the dissipation inequality (13) can be represented in the form

$$\gamma = \rho_0\dot{\psi}^c - \rho_0\eta\dot{\vartheta} - \mathrm{tr}(\dot{\boldsymbol{\sigma}}^{\mathrm{T}}\boldsymbol{\varepsilon}) - \frac{(\mathrm{grad}\vartheta)^{\mathrm{T}}}{\vartheta}\boldsymbol{q} \geqslant 0. \tag{15}$$

Developing the material time derivative of ψ^c and introducing the notations

$$\boldsymbol{Y} = \rho_0\frac{\partial\psi^c}{\partial\boldsymbol{D}}, \quad \boldsymbol{K} = -\rho_0\frac{\partial\psi^c}{\partial\boldsymbol{\kappa}}, \tag{16}$$

yields

$$\gamma = \vartheta\left(\rho_0\frac{\partial\psi^c}{\partial\vartheta} - \rho_0\eta\right) + \mathrm{tr}\left[\dot{\boldsymbol{\sigma}}^{\mathrm{T}}\left(\rho_0\frac{\partial\psi^c}{\partial\boldsymbol{\sigma}} - \boldsymbol{\varepsilon}\right)\right] + \mathrm{tr}(\boldsymbol{Y}^{\mathrm{T}}\dot{\boldsymbol{D}}) - \mathrm{tr}(\boldsymbol{K}^{\mathrm{T}}\dot{\boldsymbol{\kappa}}) - \boldsymbol{q}^{\mathrm{T}}\frac{\mathrm{grad}\vartheta}{\vartheta} \geqslant 0. \tag{17}$$

The specific Gibbs free energy describes the reversible part of the material behaviour in terms of the state variables $\mathscr{S} = (\vartheta, \boldsymbol{\sigma}, \boldsymbol{D}, \boldsymbol{\kappa})$, whereas the irreversible part of the material behaviour is dealt with the dissipation potential $\varphi = \varphi(\mathscr{W}; \mathscr{S})$ in terms of the variables of dissipation $\mathscr{W} = (\dot{\vartheta}, \boldsymbol{q}, \boldsymbol{Y}, \boldsymbol{K})$. By (Frémond, 2002), the dissipation potential has the following properties.

(i) It is a convex function from a linear space into $\bar{\mathbb{R}} = \mathbb{R} \cup \{+\infty\}$.
(ii) It is subdifferentiable function such that $\mathscr{B} \in \partial\varphi|_{\mathscr{W}}$, i.e. the subdifferential $\partial\varphi|_{\mathscr{W}}$ is a set of all subgradients $\mathscr{B} = (B_\vartheta, \boldsymbol{B}_q, \boldsymbol{B}_Y, \boldsymbol{B}_K)$. If φ is smooth, $\mathscr{B} = \partial\varphi/\partial\mathscr{W}$.
(iii) The components of $\mathscr{B}$ are members of the dual space of $\mathscr{W}$.

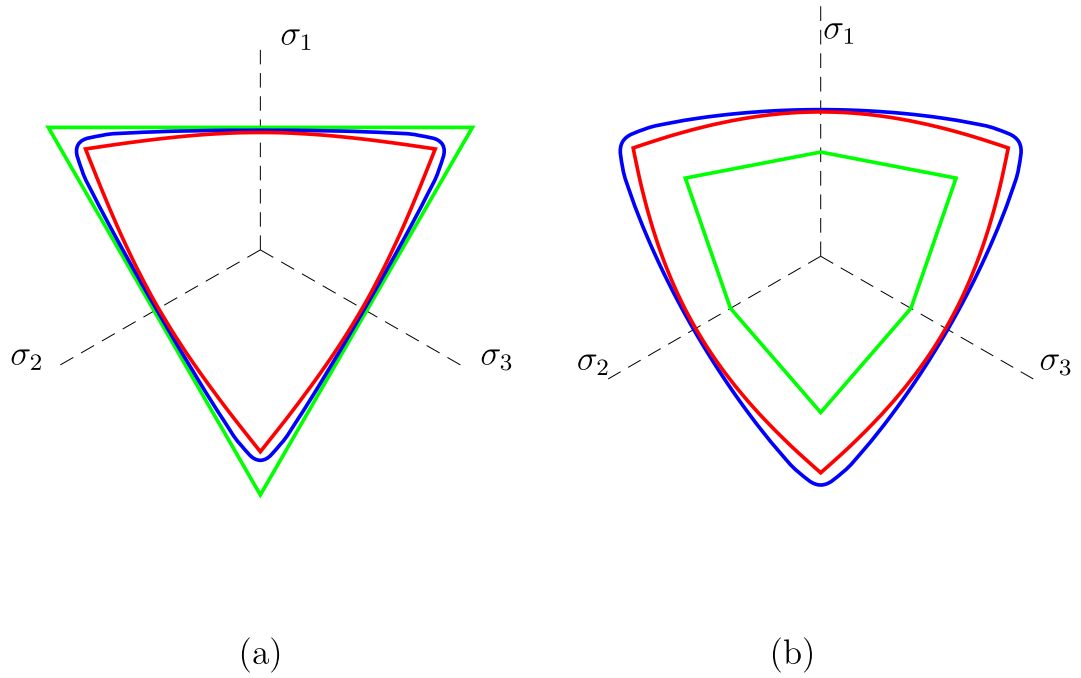

Fig. 1. Graph of three failure criteria in the π-plane (a) and in the deviatoric plane as $\sigma_m = \sigma_c$ (b). The Ottosen criterion is shown in blue, the Mohr–Coulomb criterion with tension cut-off in green and the Barcelona criterion in red ($\sigma_m = \frac{1}{3}I_1$). (For interpretation of the references to colour in this figure legend, the reader is referred to the web version of this article.)

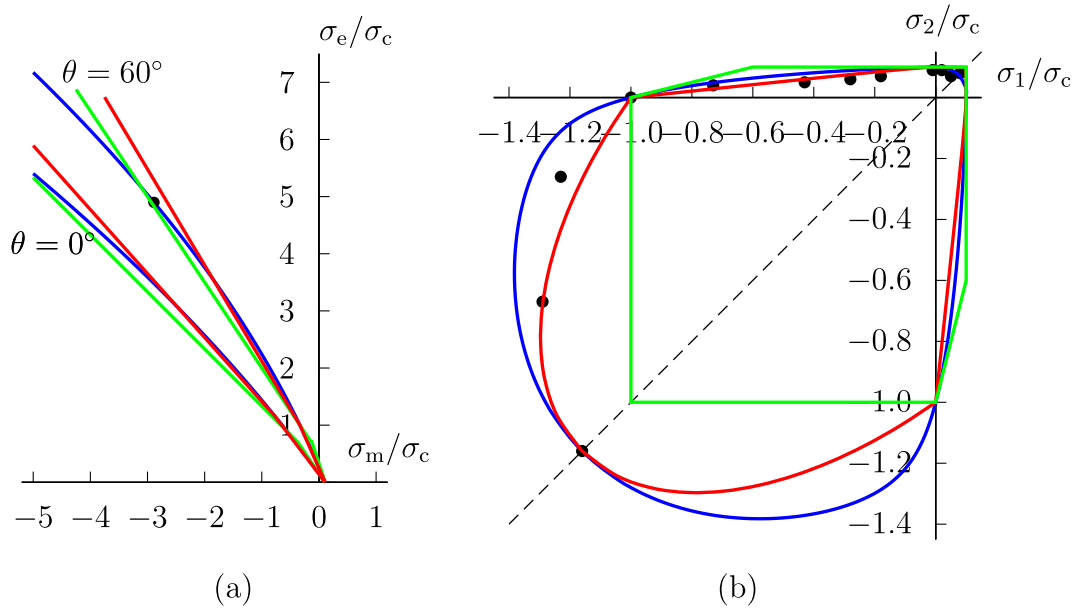

Fig. 2. Graph of three failure criteria in the meridian plane (a) and in plane stress (b). The Ottosen criterion is shown in blue, the Mohr–Coulomb criterion with tension cut-off in green and the Barcelona criterion in red. Black dots indicate the experimental results by Kupfer et al. (1969), ($\sigma_m = \frac{1}{3}I_1, \sigma_e = \sqrt{3J_2}$).

(iv) Based on the properties (i)–(iii), the product of $\mathscr{W}$ and $\mathscr{B}$ defines the power of dissipation such that

$$\gamma \equiv \dot{\vartheta} B_\vartheta + \boldsymbol{q}^{\mathrm{T}} \boldsymbol{B}_q + \mathrm{tr}(\boldsymbol{Y}^{\mathrm{T}} \boldsymbol{B}_Y) + \mathrm{tr}(\boldsymbol{K}^{\mathrm{T}} \boldsymbol{B}_K). \tag{18}$$

Properties (i) and (ii) provide information to formulate the dissipation potential for dealing with constraints such as failure criteria due to non-smooth material behaviour, and based on property (i), $\mathscr{W}\mathscr{B} \geqslant 0$ for all $\mathscr{W}$ and $\mathscr{B}$.

Equating the definition (18) with the dissipation power in (17) results in equation

$$\dot{\vartheta}\left(\rho_0 \frac{\partial \psi^{\mathrm{c}}}{\partial \vartheta} - \rho_0 \eta - B_\vartheta\right) + \mathrm{tr}\left[\dot{\boldsymbol{\sigma}}^{\mathrm{T}}\left(\rho_0 \frac{\partial \psi^{\mathrm{c}}}{\partial \boldsymbol{\sigma}} - \boldsymbol{\varepsilon}\right)\right] + \boldsymbol{q}^{\mathrm{T}}\left(-\frac{\mathrm{grad}\vartheta}{\vartheta} - \boldsymbol{B}_q\right) + \mathrm{tr}\left[\boldsymbol{Y}^{\mathrm{T}}(\dot{\boldsymbol{D}} - \boldsymbol{B}_Y)\right] + \mathrm{tr}\left[\boldsymbol{K}^{\mathrm{T}}(-\dot{\boldsymbol{\kappa}} - \boldsymbol{B}_K)\right] = 0. \tag{19}$$

Eq. (19) holds for arbitrary $\mathscr{W}$ only, if the coefficients in brackets () tend to zero, i.e.

$$\rho_0 \frac{\partial \psi^{\mathrm{c}}}{\partial \vartheta} - \rho_0 \eta - B_\vartheta = 0, \tag{20}$$

$$\rho_0 \frac{\partial \psi^{\mathrm{c}}}{\partial \boldsymbol{\sigma}} - \boldsymbol{\varepsilon} = 0, \tag{21}$$

$$-\frac{\operatorname{grad}\vartheta}{\vartheta} - \boldsymbol{B}_q = 0, \tag{22}$$

$$\dot{\boldsymbol{D}} - \boldsymbol{B}_Y = 0, \tag{23}$$

$$-\dot{\boldsymbol{\kappa}} - \boldsymbol{B}_K = 0. \tag{24}$$

If these equations hold for any physical process that satisfy the balance equations of momentum and energy, the dissipation inequality (15) is satisfied. Then Eqs. (20)–(24) are, by definition, thermodynamically admissible.

3.2. Specific model

In this work, it is assumed that an undamaged body behaves like a linear elastic solid, deformations are fully elastic, and the material failure results from anisotropic damage with an isotropic hardening–softening feature.

Assuming that the mechanical and thermal behaviour are uncoupled and that the hardening–softening property is independent of the damage and stresses, the specific Gibbs free energy function can be decomposed into three parts as

$$\psi^{\mathrm{c}}(\vartheta, \boldsymbol{\sigma}, \boldsymbol{D}, \kappa) = \psi_1^{\mathrm{c}}(\vartheta) + \psi_2^{\mathrm{c}}(\boldsymbol{\sigma}, \boldsymbol{D}) + \psi_3^{\mathrm{c}}(\kappa). \tag{25}$$

Since thermal effects have no role in the mechanical behaviour that is the main concern of this work, $\psi_1^{\mathrm{c}}(\vartheta)$ is left unspecified.

Assuming that ψ_2^{c} is a scalar-valued isotropic function such that $\psi_2^{\mathrm{c}}(\boldsymbol{\sigma}, \boldsymbol{D}) = \psi_2^{\mathrm{c}}(\boldsymbol{Q}\boldsymbol{\sigma}\boldsymbol{Q}^{\mathrm{T}}, \boldsymbol{Q}\boldsymbol{D}\boldsymbol{Q}^{\mathrm{T}})$, where $\boldsymbol{Q}$ is a proper orthogonal second order tensor, it can be formulated by applying the integrity basis for $\boldsymbol{\sigma}$ and $\boldsymbol{D}$

$$\left\{\operatorname{tr}\boldsymbol{\sigma}, \operatorname{tr}(\boldsymbol{\sigma}^2), \operatorname{tr}(\boldsymbol{\sigma}^3), \operatorname{tr}\boldsymbol{D}, \operatorname{tr}(\boldsymbol{D}^2), \operatorname{tr}(\boldsymbol{D}^3), \operatorname{tr}(\boldsymbol{\sigma}\boldsymbol{D}), \operatorname{tr}(\boldsymbol{\sigma}\boldsymbol{D}^2), \operatorname{tr}(\boldsymbol{\sigma}^2\boldsymbol{D}), \operatorname{tr}(\boldsymbol{\sigma}^2\boldsymbol{D}^2)\right\}. \tag{26}$$

Using the terms of (26) that are linear in $\boldsymbol{D}$ for damage and quadratic in $\boldsymbol{\sigma}$ for linear elasticity, the specific Gibbs free energy sub-function representing the damage-degrading elastic behaviour is defined as

$$\psi_2^{\mathrm{c}}(\boldsymbol{\sigma}, \boldsymbol{D}) = \frac{1}{\rho_0}\left\{\frac{1}{4G}[\operatorname{tr}(\boldsymbol{s}^2) + \operatorname{tr}(\boldsymbol{s}^2\boldsymbol{D})] + \frac{1}{18K_{\mathrm{b}}}(1 + \chi \operatorname{tr}\boldsymbol{D})(\operatorname{tr}\boldsymbol{\sigma})^2\right\} \tag{27}$$

where G and K_{b} stand for the shear and bulk modulus, χ is a dimensionless positive material parameter. It can be noticed that for isotropic damage, i.e. when $\boldsymbol{D} = D\boldsymbol{I}$, where D is the scalar damage variable, and selecting $\chi = \frac{1}{3}$, the free energy (27) reduces to the standard scalar isotropic damage format

$$\psi_2^{\mathrm{c}} = \frac{1}{\rho_0}(1 + D)[\frac{1}{4G}\operatorname{tr}(\boldsymbol{s}^2) + \frac{1}{18K_{\mathrm{b}}}(\operatorname{tr}\boldsymbol{\sigma})^2]. \tag{28}$$

The damage tensor $\boldsymbol{D}$ is closely related to the crack density tensor by Kachanov (1992).

The third part of the specific Gibbs free energy describes the energy stored within the body due to hardening and softening of the material. It is defined by the integral

$$\psi_3^{\mathrm{c}}(\kappa) = \frac{1}{\rho_0}\int_0^{\kappa}\int_0^{\kappa'} g(\kappa'')\mathrm{d}\kappa''\mathrm{d}\kappa', \tag{29}$$

where the integrand $g(\kappa)$ is a four-parameter rational function formulated as

$$g(\kappa) = \frac{H_0}{\kappa_0}\frac{h_2(\kappa/\kappa_0)^2 - 2h_1(\kappa/\kappa_0) - 1}{\left[h_2(\kappa/\kappa_0)^2 + 1\right]^2}. \tag{30}$$

It characterises the non-linear response of the material to the internal variable κ as illustrated in Fig. 3a. The initial hardening modulus H_0 and dimensionless parameters κ_0, h_1 and h_2 are determined in the following section.

To formulate the irreversible behaviour of the body the dissipation potential is defined by the thermodynamic forces $\boldsymbol{Y}$ and K describing the damage and hardening, respectively. Furthermore, thermal coupling is omitted by restriction to isothermal cases. The dissipation potential is now given as

$$\varphi(\boldsymbol{Y}, K; \boldsymbol{\sigma}, \boldsymbol{\varepsilon}) = \mathrm{I}(\boldsymbol{Y}, K; \boldsymbol{\sigma}, \boldsymbol{\varepsilon}), \tag{31}$$

where I denotes the indicator function that handles the given constraint. By Frémond (2002), it is defined as

$$\mathrm{I}(\boldsymbol{Y}, K; \boldsymbol{\sigma}, \boldsymbol{\varepsilon}) = \begin{cases} 0, & \text{if} \quad (\boldsymbol{Y}, K) \in \Sigma \\ +\infty, & \text{if} \quad (\boldsymbol{Y}, K) \notin \Sigma, \end{cases} \tag{32}$$

where Σ is a convex set determining the admissible domains for $\boldsymbol{Y}$ and K. This set is defined by means of the damage criterion $f(\boldsymbol{Y}, K; \boldsymbol{\sigma}, \boldsymbol{\varepsilon}) \leqslant 0$ such that

$$\Sigma = \left\{(\boldsymbol{Y}, K) \in \mathbb{R}^6 \times \mathbb{R} \mid f(\boldsymbol{Y}, K; \boldsymbol{\sigma}, \boldsymbol{\varepsilon}) \leqslant 0\right\}. \tag{33}$$

Furthermore, the subdifferential of I is defined as

$$\partial \mathrm{I} = \begin{cases} \left\{(\boldsymbol{B}_Y, B_K) \in \mathbb{R}^6 \times \mathbb{R} \mid (\boldsymbol{B}_Y, B_K) = (\boldsymbol{0}, 0), \quad \text{if} \quad f < 0; \right. \\ \left. (\boldsymbol{B}_Y, B_K) = (\dot{\lambda}\frac{\partial f}{\partial \boldsymbol{Y}}, \dot{\lambda}\frac{\partial f}{\partial K}), \ \dot{\lambda} \geqslant 0, \quad \text{if} \quad f = 0\right\}, \quad \text{if} \quad (\boldsymbol{Y}, K) \in \Sigma \\ \varnothing, \quad \text{if} \quad (\boldsymbol{Y}, K) \notin \Sigma. \end{cases} \tag{34}$$

Since the failure modes of deformation are essential, the damage surface is now formulated as

$$f(\boldsymbol{Y}, K; \boldsymbol{\sigma}, \boldsymbol{\varepsilon}) = \frac{AJ_2}{\sigma_{\mathrm{c}}} + \Lambda\sqrt{J_2} + BI_1 - (\sigma_{\mathrm{c0}} + K) + \operatorname{tr}\left[\boldsymbol{A}^{\mathrm{T}}(\boldsymbol{Y} - \boldsymbol{Y}(\boldsymbol{\sigma}))\right], \tag{35}$$

where $\boldsymbol{A} = \boldsymbol{A}(\boldsymbol{\sigma}, \boldsymbol{\varepsilon})$ is a symmetric positive definite second-order tensor defined as

$$\boldsymbol{A}(\boldsymbol{\sigma}, \boldsymbol{\varepsilon}) = \frac{1}{1 + \beta_1\langle \operatorname{tr}\boldsymbol{\sigma}\rangle/\sigma_{\mathrm{t}}}\left(\frac{\boldsymbol{\varepsilon}_+}{\|\boldsymbol{\varepsilon}_+\|} + \beta_2\boldsymbol{I}\right) \tag{36}$$

and $\boldsymbol{\varepsilon}_+$ is the positive part of the elastic strain tensor, i.e.

$$\boldsymbol{\varepsilon}_+ = \sum_{i=1}^{3}\langle\varepsilon_i\rangle\boldsymbol{\phi}_i \otimes \boldsymbol{\phi}_i, \tag{37}$$

where $\varepsilon_i,\ i = 1, \ldots, 3$ are the eigenvalues of the elastic strain tensor, $\boldsymbol{\phi}_i$ stands for the corresponding eigenvectors and β_1, β_2 are positive parameters. The norm of a second order tensor tensor is defined in a standard way, i.e. $\|\boldsymbol{\varepsilon}_+\| = \sqrt{\operatorname{tr}(\boldsymbol{\varepsilon}_+^2)}$, and $\langle\bullet\rangle$ denotes the Macaulay brackets. If all eigenvalues ε_i are negative, the term $\boldsymbol{\varepsilon}_+/\|\boldsymbol{\varepsilon}_+\|$ is neglected in the expression of $\boldsymbol{A}$.

Use of the ramp function $\langle\bullet\rangle$ can produce discontinuities of the derivatives which might result in divergence of the local iteration if standard Newton scheme is applied. A simple way to avoid these convergence problems is to use a smooth approximation for the ramp function e.g. $\langle x\rangle \approx \frac{1}{2}x(1 + x/\sqrt{x^2 + \delta^2})$, where δ is a small parameter.

The damage surface (35) should be a function of the thermodynamic force $\boldsymbol{Y}$ to obtain the evolution equations for the damage. It is possible to express the stress invariants I_1, J_2 and $\cos 3\theta$ in the Ottosen failure criterion in terms of $\boldsymbol{Y}$, however, such relations are not unique. One alternative is presented in Yaghoubi et al. (2014). In the present study, the failure criterion of Ottosen is kept untouched and expressed in terms of stress, which acts as a parameter in the dissipation potential, and a zero term linear in $\boldsymbol{Y}$ is

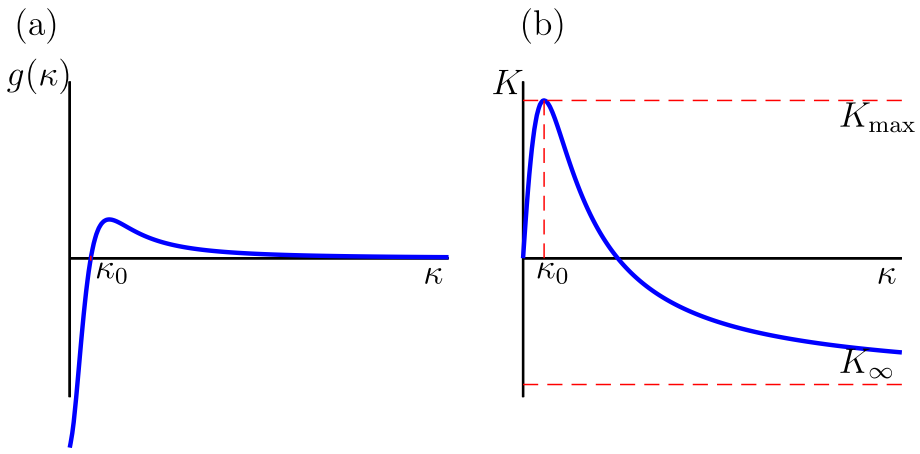

Fig. 3. (a) Response of material to the hardening variable κ. (b) Hardening variable K.

added. The dissipation inequality is automatically satisfied if the tensor $\boldsymbol{A}$ is symmetric positive definite.

The thermodynamic force $\boldsymbol{Y}$ dual to the damage rate is obtained from definitions $(16)_1$ and (27) as a function of stress

$$\boldsymbol{Y}(\boldsymbol{\sigma}) = \frac{1}{4G}\boldsymbol{s}^2 + \frac{\chi}{18K_\mathrm{b}}(\mathrm{tr}\,\boldsymbol{\sigma})^2\boldsymbol{I}. \tag{38}$$

By definition $(16)_2$, the hardening variable K obtains the form

$$K = -\int_0^\kappa g(\kappa')\mathrm{d}\kappa' = H_0\frac{h_1(\kappa/\kappa_0)^2 + (\kappa/\kappa_0)}{h_2(\kappa/\kappa_0)^2 + 1}, \tag{39}$$

which is illustrated in Fig. 3b.

Positive definiteness of tensor $\boldsymbol{A}$ in (35) together with the requirement that $\chi \geqslant 0$ in (38) guarantees that the dissipation power (18) is non-negative.

Using Eqs. (21), (23) and (24) together with definitions (25), (27), (32), (31) and (34), yields the following constitutive equations representing the mechanical behaviour of an elastic-brittle body. For the damage degrading elastic deformations it is obtained

$$\boldsymbol{\varepsilon} = \frac{1}{2G}\left[\boldsymbol{s} + \frac{1}{2}(\boldsymbol{s}\boldsymbol{D} + \boldsymbol{D}\boldsymbol{s}) - \frac{1}{3}\mathrm{tr}(\boldsymbol{s}\boldsymbol{D})\boldsymbol{I}\right] + \frac{1}{9K_\mathrm{b}}(1 + \chi\mathrm{tr}\boldsymbol{D})(\mathrm{tr}\boldsymbol{\sigma})\boldsymbol{I}. \tag{40}$$

The evolution of internal variables describing damage and hardening is governed by equations

$$\dot{\mathbf{D}} = \dot{\lambda}\frac{\partial f}{\partial \boldsymbol{Y}} = \dot{\lambda}\boldsymbol{A}(\boldsymbol{\sigma},\boldsymbol{\varepsilon}) = \frac{\dot{\lambda}}{1 + \beta_1\langle\mathrm{tr}\,\boldsymbol{\sigma}\rangle/\sigma_\mathrm{t}}\left(\frac{\boldsymbol{\varepsilon}_+}{\|\boldsymbol{\varepsilon}_+\|} + \beta_2\boldsymbol{I}\right), \tag{41}$$

$$\dot{\kappa} = -\dot{\lambda}\frac{\partial f}{\partial K} = \dot{\lambda}. \tag{42}$$

The multiplier $\dot{\lambda}$ in (41) and (42) can be determined by the consistency condition

$$\dot{f}(\boldsymbol{Y}, K; \boldsymbol{\sigma}, \boldsymbol{\varepsilon}) = 0. \tag{43}$$

It can be easily seen that the failure mode is correct in unconfined uniaxial tension and compression. In the uniaxial tension in the 11-direction, it results in the damage rate

$$\dot{\mathbf{D}} \sim \begin{pmatrix} 1+\beta_2 & 0 & 0 \\ 0 & \beta_2 & 0 \\ 0 & 0 & \beta_2 \end{pmatrix}, \tag{44}$$

and in the uniaxial compression in the 11-direction, it gives

$$\dot{\mathbf{D}} \sim \begin{pmatrix} \beta_2 & 0 & 0 \\ 0 & 1+\beta_2 & 0 \\ 0 & 0 & 1+\beta_2 \end{pmatrix}. \tag{45}$$

Since β_2 is positive, axial splitting mode in compression is thus properly modelled.

3.3. Determination of material parameters

Parameters A, B, k_1 and k_2 in the failure surface are adjusted to represent the damage surface corresponding with the failure states (i)–(iv) in Section 2. Substituting the values for $\sigma_\mathrm{c}, \sigma_\mathrm{t}, \sigma_\mathrm{bc}$ and the stress on the compressive meridian in Eqs. (5)–(8) result the values for A, B, k_1 and k_2. It can be seen that the damage criterion (35) represents correctly the ultimate stress states when $K = K_{\max} = \sigma_\mathrm{c} - \sigma_{\mathrm{c}0}$.

To obtain the parameters χ, κ_0, β_1 and β_2, the uniaxial compression and tension as well as the biaxial test results are needed.

The isotropic part on the damage evolution is governed by the β_2-parameter. It can be found together with the χ-parameter from the secant-modulus in loading and transverse directions considering both uniaxial and biaxial compression cases. In the unconfined uniaxial stress state $\sigma_{11} \neq 0$, Eq. (40) gives the strains

$$\begin{cases} \varepsilon_{11} = \frac{\sigma_{11}}{E}\left[1 + \left(\frac{4}{9}(1+\nu) + \frac{1}{3}(1-2\nu)\chi\right)D_{11} + \frac{2}{3}\left(\frac{1}{3}(1+\nu) + (1-2\nu)\chi\right)D_{22}\right], \\ \varepsilon_{22} = \frac{\sigma_{11}}{E}\left[-\nu - \frac{1}{3}\left(\frac{2}{3}(1+\nu) - (1-2\nu)\chi\right)D_{11} - \frac{1}{3}\left(\frac{1}{3}(1+\nu) - 2(1-2\nu)\chi\right)D_{22}\right], \end{cases} \tag{46}$$

where it has been taken into account that $D_{33} = D_{22}$ according to (41). The ratio between the damage values in the loading and transverse directions in the unconfined uniaxial compression test is

$$\frac{D_{11}}{D_{22}} = \frac{\sqrt{2}\beta_2}{1 + \sqrt{2}\beta_2} = \beta_\mathrm{c}. \tag{47}$$

Taking this into account, expressions for the strain components (46) can be written in a more simple form

$$\begin{cases} \varepsilon_{11} = \frac{\sigma_{11}}{E}(1 + a_{11,\mathrm{c}}D_{22}), \\ \varepsilon_{22} = -\frac{\sigma_{11}}{E}(\nu + a_{22,\mathrm{c}}D_{22}), \end{cases} \tag{48}$$

where

$$\begin{cases} a_{11,\mathrm{c}} = \frac{1}{3}\left[\frac{2}{3}(1+\nu) + 2(1-2\nu)\chi + \beta_\mathrm{c}\left(\frac{4}{3}(1+\nu) + (1-2\nu)\chi\right)\right], \\ a_{22,\mathrm{c}} = \frac{1}{3}\left[\frac{1}{3}(1+\nu) - 2(1-2\nu)\chi + \beta_\mathrm{c}\left(\frac{2}{3}(1+\nu) - (1-2\nu)\chi\right)\right]. \end{cases} \tag{49}$$

The secant modules in the uniaxial compression case are

$$\begin{cases} E_{\mathrm{c},1,\mathrm{sec}} = \frac{\sigma_\mathrm{c}}{|\varepsilon_{11,\mathrm{c}}|} = \frac{E}{1 + a_{11,\mathrm{c}}D_{22,\mathrm{c}}}, \\ E_{\mathrm{c},2,\mathrm{sec}} = \frac{\sigma_\mathrm{c}}{|\varepsilon_{22,\mathrm{c}}|} = \frac{E}{\nu + a_{22,\mathrm{c}}D_{22,\mathrm{c}}}. \end{cases} \tag{50}$$

Evaluating the secant modules at the peak load $\sigma_{11} = -\sigma_c$ yields equation

$$D_{22,c} = \frac{1}{a_{11,c}}\left(\frac{E \mid \varepsilon_{11,c} \mid}{\sigma_c} - 1\right) = \frac{1}{a_{22,c}}\left(\frac{E \mid \varepsilon_{22c} \mid}{\sigma_c} - v\right) \tag{51}$$

relating the two unknown material parameters χ and β_2.

In the equibiaxial compressive stress state, where $\sigma_{11} = \sigma_{22} = \sigma$, expressions for the strain components are

$$\begin{cases} \varepsilon_{11} = \frac{\sigma}{E}(1 - v + a_{11,bc}D_{33}), \\ \varepsilon_{33} = \frac{\sigma}{E}(-2v - a_{33,bc}D_{33}), \end{cases} \tag{52}$$

where

$$\begin{cases} a_{11,bc} = \frac{1}{3}\left[\frac{2}{3}(1+v) + 2(1-2v)\chi + \beta_{bc}\left(\frac{1}{3}(1+v) + 4(1-2v)\chi\right)\right], \\ a_{33,bc} = \frac{1}{3}\left[\frac{4}{3}(1+v) - 2(1-2v)\chi - \beta_{bc}\left(\frac{2}{3}(1+v) + (1-2v)\chi\right)\right], \end{cases} \tag{53}$$

and

$$\beta_{bc} = \frac{D_{11}}{D_{33}} = \frac{\beta_2}{1+\beta_2}. \tag{54}$$

The secant modules at the peak stress $\sigma = -\sigma_{bc}$ results in the expressions

$$\begin{cases} E_{bc,1,sec} = \frac{\sigma_{bc}}{|\varepsilon_{11,bc}|} = \frac{E}{1 - v + a_{11,c}D_{33,c}}, \\ E_{bc,3,sec} = \frac{\sigma_{bc}}{|\varepsilon_{22,c}|} = \frac{E}{2v + a_{33,c}D_{33,c}}. \end{cases} \tag{55}$$

Solving the dominant damage component from Eqs. (55) gives the second equation relating the material parameters χ and β_2

$$D_{33,bc} = \frac{1}{a_{11,bc}}\left(\frac{E \mid \varepsilon_{11,bc} \mid}{\sigma_{bc}} - 1 + v\right) = \frac{1}{a_{33,bc}}\left(\frac{E \mid \varepsilon_{33,bc} \mid}{\sigma_{bc}} - 2v\right). \tag{56}$$

Eqs. (51) and (56) form a system

$$\begin{cases} u_0 + 2u_0\beta_c - u_1(2 + \beta_c)\chi = 0, \\ b_0 - b_1\beta_c - b_2(1 + 2\beta_{bc})\chi = 0, \end{cases} \tag{57}$$

where

$$\begin{cases} u_0 = \frac{1}{3}(1+v)(\phi_1 - 2\phi_2), \\ u_1 = (1-2v)(\phi_1 + \phi_2), \\ b_0 = \frac{2}{9}(1+v)(2\phi_3 - \phi_4), \\ b_1 = \frac{1}{9}(1+v)(2\phi_3 + \phi_4), \\ b_2 = \frac{2}{3}(1-2v)(\phi_3 - \phi_4), \\ \phi_1 = E\varepsilon_c/\sigma_c - 1, \\ \phi_2 = E\varepsilon_{22,c}/\sigma_c - v, \\ \phi_3 = E\varepsilon_{11,bc}/\sigma_{bc} - 1 + v, \\ \phi_4 = E\varepsilon_{33,bc}/\sigma_{bc} - 2v. \end{cases} \tag{58}$$

Eliminating χ from the system (57) and taking definitions (47) and (54) into account, results in the quadratic equation for β_2

$$a_2\beta_2^2 + a_1\beta_2 + a_0 = 0, \tag{59}$$

where

$$\begin{cases} a_2 = \sqrt{2}(9\tilde{u} - 3(1-\xi)\tilde{b}), \\ a_1 = 3(1+\sqrt{2})\tilde{u} - [3\sqrt{2} + 2(1-\xi)]\tilde{b}, \\ a_0 = \tilde{u} - 2\tilde{b}, \\ \tilde{u} = u_0/u_1, \quad \tilde{b} = b_0/b_2, \quad \xi = b_1/b_0. \end{cases} \tag{60}$$

The parameters H_0, κ_0, h_1 and h_2 in the hardening function (39) are determined in terms of the maximum and limit ($\kappa \to \infty$) values of K i.e. $K_{max} = \sigma_c - \sigma_{c0}$ and K_∞. On the condition that $g(\kappa) = 0$ for $\kappa = \kappa_0$, Eq. (30) yields the equation

$$h_2 - 2h_1 - 1 = 0, \tag{61}$$

and, by (39), K obtains its maximum value

$$K_{max} = K(\kappa_0) = H_0\frac{h_1 + 1}{h_2 + 1}. \tag{62}$$

Furthermore, for $\kappa \to \infty, K$ obtains its limit value

$$K_\infty = H_0\frac{h_1}{h_2}. \tag{63}$$

Combining Eqs. (61)–(63) leads to

$$H_0 = 2K_{max}, \tag{64}$$

$$h_1 = \frac{\frac{1}{2}K_\infty}{K_{max} - K_\infty}, \tag{65}$$

$$h_2 = \frac{K_{max}}{K_{max} - K_\infty}. \tag{66}$$

The κ_0-parameter is defined as the value for the internal variable κ at the peak stress in the uniaxial compression test where $\sigma_{11} = -\sigma_c$. From (41), (42) and utilizing (47) it is obtained

$$\dot{\kappa} = \dot{\lambda} = \frac{1}{\sqrt{1 + 2\beta_2\mathrm{tr}(\boldsymbol{\varepsilon}_+)/\|\boldsymbol{\varepsilon}_+\| + 3\beta_2^2}}\|\dot{\mathbf{D}}\|. \tag{67}$$

Using Eqs. (51) and (67) the value for κ_0 can be obtained as

$$\kappa_0 = \frac{\sqrt{2}}{1 + \sqrt{2}\beta_2}D_{22,c} = \kappa_c D_{22,c}. \tag{68}$$

Using a point in the strain-softening post-peak region, K_∞ can be determined by using Eq. (51) at the post-peak point on the uniaxial compression stress–strain curve

$$D_{22,pp} = \frac{1}{a_{11,c}}\left(\frac{E \mid \varepsilon_{11,pp} \mid}{\mid \sigma_{pp} \mid} - 1\right). \tag{69}$$

The hardening variable at that point is obtained from (68) as

$$\kappa_{pp} = \kappa_c D_{22,pp}. \tag{70}$$

Substituting this value to the expression of the hardening parameter and to the damage criterion (35)

$$\hat{f}(\sigma_{pp}) - (\sigma_{c0} + K(\kappa_{pp})) = 0, \tag{71}$$

from which the K_∞ can be solved as

$$K_\infty = K_{max}\frac{((\kappa_{pp}/\kappa_0)^2 + 1)(\hat{f}(\sigma_{pp}) - \sigma_{c0})/H_0 - \kappa_{pp}/\kappa_0}{(\kappa_{pp}/\kappa_0)(\kappa_{pp}/(2\kappa_0) - 1) + (\hat{f}(\sigma_{pp}) - \sigma_{c0})/H_0} \tag{72}$$

and where $\hat{f} = f + (\sigma_{c0} + K)$.

The remaining β_1 parameter is obtained from the tensile test data. In the uniaxial tensile test the ratio between damage components is

$$\frac{D_{22}}{D_{11}} = \frac{\beta_2}{1+\beta_2}, \tag{73}$$

which results in the maximum value for the dominant damage component

$$D_{11,t} = \frac{1}{a_{11,t}}\left(\frac{E\varepsilon_t}{\sigma_t} - 1\right), \tag{74}$$

where

$$a_{11,t} = \frac{1}{3}\left[\frac{4}{3}(1+v) + (1-2v)\chi + \frac{2\beta_2}{1+\beta_2}\left(\frac{1}{3}(1+v) + (1-2v)\chi\right)\right]. \tag{75}$$

The damage value at the tensile strength (74) can be written also as

$$D_{11,t} = \frac{1}{a_{11,t}}\left(\frac{E\mid \varepsilon_t \mid}{\sigma_t} - 1\right) = \kappa_0 \frac{1+\beta_2}{1+\beta_1}, \tag{76}$$

from which the β_1 can be solved as

$$\beta_1 = (1+\beta_2)\frac{\kappa_0}{D_{11,t}}. \tag{77}$$

4. Results

The model has been implemented in a strain-driven code using implicit Euler integration. A short description of the solution procedure is given in Appendix.

For assessing the quality of the proposed model, the model predictions are compared to the well documented experimental data for concrete by Kupfer et al. (1969) and the values needed to calibrate the present model are shown in Table 1. Kupfer et al. (1969) performed the biaxial tests with specimens having dimensions 20 cm × 20 cm × 5 cm and the model results are compared to the tests having unconfined uniaxial compressive strength of 30.9 MPa, maximum aggregate size 15 mm and the water-cement ratio 0.9. The resulted parameters for the present model are shown in Table 2.

Four loading cases are considered: (i) unconfined uniaxial compression, (ii) unconfined uniaxial tension, (iii) equibiaxial compression and (iv) biaxial compression with stress ratio $\sigma_{11}/\sigma_{22} = -1/-0.52$. Assuming that, in each loading case, the concrete is in an uniform state, the response of the concrete to the loading can be defined uniformly by the equations of the constitutive model considering only one material point.

Materials like concrete, natural rocks and natural ice are heterogeneous containing pores and flaws and other weaknesses exhibiting variation in compressive and tensile strengths. In the simulations, the material heterogeneity can be considered by varying material parameters of the model; e.g. assuming that both the compressive and tensile strength have spatial random field fluctuation with specific probabilistic distribution, see also Benkemoun et al. (2010), Mondal et al. (2019). As shown by Kolari (2017) in uniaxial compression simulations of natural ice, the material parameter variation induced non-simultaneous damage evolution and variation in strength, but did not affect to the macroscopic splitting failure mode.

For comparison, computations with the Concrete Damaged Plasticity (CDP) model available in the commercial finite element software Abaqus (Dassault Systémes, 2020) have been carried out for uniaxial and equibiaxial compression cases. The CDP model is based on the works by Lubliner et al. (1989), Lee (1996) and Lee and Fenves (1998). In this model, a scalar damage parameter is used to describe stiffness degradation while the plastic behaviour is formulated with a non-assosiative Drucker-Prager type yield function with tension cut-off. The adopted flow rule is based on the Mohr–Coulomb like flow rule approach.

Table 1
Material data from Kupfer et al. (1969). Notice that the strain values $\varepsilon_{11,c}$ etc. are absolute values and should be used as such in equations of Section 3.3.

Quantity	Value	Unit	Notes
E	31.9	GPa	
ν	0.2	–	
σ_c	30.9	MPa	
σ_t	2.78	MPa	
σ_{bc}	35.8	MPa	
$I_{1,4}$	−267.6	MPa	Ottosen and Ristinmaa (2005)
$\sqrt{J_{2,4}}$	87.4	MPa	Ottosen and Ristinmaa (2005)
σ_{c0}	10.8	MPa	$0.35\sigma_c$
$\varepsilon_{11,c}$	0.0022	–	
$\varepsilon_{22,c}$	0.000806	–	
$\varepsilon_{11,t}$	0.00009	–	
$\varepsilon_{11,bc}$	0.0026	–	
$\varepsilon_{33,bc}$	0.0033	–	
σ_{pp}	26.282	MPa	
$\varepsilon_{11,pp}$	0.0031887	–	

Table 2
Model parameters calculated from the material data in Table 1.

Quantity	Value	Unit	Notes
A	1.512	–	
B	3.597	–	
k_1	12.963	–	
k_2	0.9864	–	
K_∞	−6.72	MPa	
H_0	40.2	MPa	
h_1	−0.1253	–	
h_2	0.7494	–	
κ_0	3.5151	–	
χ	0.00162	–	
β_1	75.843	–	
β_2	0.21551	–	

4.1. Unconfined uniaxial compression

The stress–strain response of concrete under unconfined uniaxial compression is shown in Fig. 4. The rate-independent Abaqus CDP model is calibrated from the experimental $\sigma_{11}, \varepsilon_{11}$ data. In addition, the dilatation angle in the plastic potential is varied using the values $2^\circ, 8^\circ, 16^\circ$ and 32°. The eccentricity parameter has been set to zero. It is clearly seen that the stress–strain response of the CDP mode in this uniaxial loading case is close to the experimental values with the dilatation angle 32°, however, this is not the case for the equibiaxial compressive loading, compare Figs. 4 and 8. In addition, the CDP model cannot predict the correct failure mode.

The damage-strain relation for the present model is shown in Fig. 5 and it is clearly seen that the mode of failure, i.e. the splitting mode is properly predicted. The ratio between the transversal and longitudinal damage is according to (47) 4.28, as it can be seen from Fig. 5. For the present model, the post-peak fitting point is the last experimental point shown in Fig. 4, having coordinates $(\varepsilon_{11}/\varepsilon_c, -\sigma_{11}/\sigma_c) = (-1.45, 0.85)$. The lateral strain ε_{22} is not developing as fast as in test, however, it should be remembered that the model solution assumes uniform strain and stress fields, which in real test cannot be obtained.

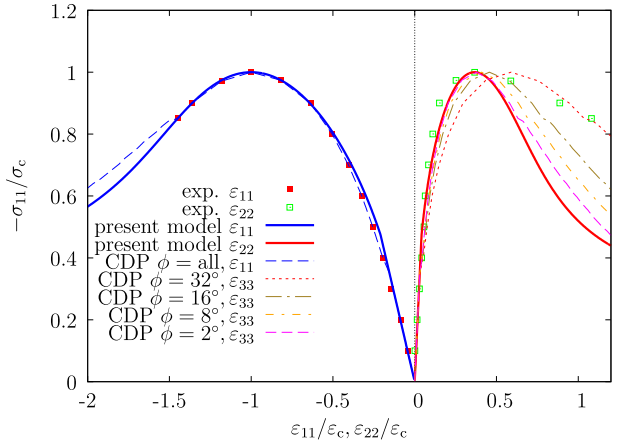

Fig. 4. Stress–strain relation in unconfined uniaxial compression. The Abaqus CDP model responses are shown for four values of the dilatation angle. Experimental data is from Kupfer et al. (1969).

4.2. Unconfined uniaxial tension

In contrast to the uniaxial compression test the fracture mode in unconfined uniaxial tension test is completely different. The damage-strain relation is shown in 6, which shows that the damage component D_{11} is 5.64 times the value of D_{22}, as it should be according to Eq. (73). This indicates that the damage grows in the direction of the tensile stress. Fig. 7 shows the calculated stress–strain response together with the experimental results. The behaviour of the model is brittle which is in line of experimental evidence for concrete under unconfined uniaxial tension.

4.3. Biaxial compression

Results for the equibiaxial compression test ($\sigma_{11} = \sigma_{22}$) are shown in Fig. 8. For the present model, correspondence to the experimental results is even better than in the unconfined uniaxial compression test. The best similarity to the experimental results for the Abaqus CDP model is obtained when the dilatation angle is 8°, in which case the $\sigma_{11}, \epsilon_{33}$-curve is almost identical to the response of the present model. However, for the CPD model the strain in the loading direction starts to deviate from the experimental results already before the peak stress.

The dominant damage develops perpendicularly to the plane of loading and the ratio $D_{33}/D_{11} = 5.64$, Eq. (54), as it can be seen from Fig. 9.

Also biaxial compression with stress ratio $\sigma_{11}/\sigma_{22} = -1/-0.52$ is analysed. Results are shown in Fig. 10. In this case the failure criterion of Ottosen overestimates the peak stress about 7 %.

5. Discussion

The proposed model utilise the failure surface of Ottosen in combination of damage description with a second order symmetric positive definite damage tensor. Despite of its simplicity, it can model well the behaviour of plain concrete both qualitatively and quantitatively. It also can predict correctly the failure mode, which many of the existing models for concrete and quasi-brittle materials in general cannot. Parameters of the model can be uniquely obtained in closed form from four different loading cases.

It is well-known that a strain-softening rate-independent material model will result in an ill-posed boundary value problem in the softening range. In the finite element analysis use of such a model produces highly mesh-dependent solutions. A simple remedy would be to make the softening material model dependent on the size of the finite element. More rigorous approaches to regular-

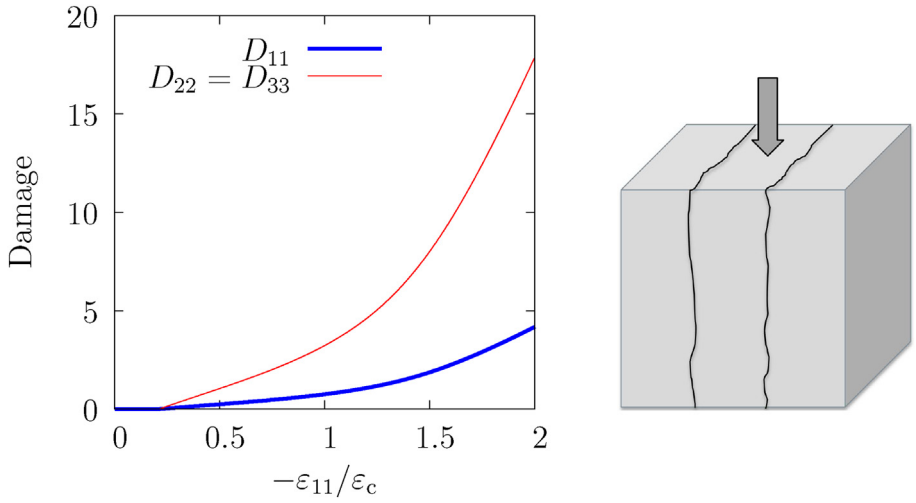

Fig. 5. Damage-strain relation in unconfined uniaxial compression. Figure on the RHS illustrates the axial splitting along the direction of uniaxial compression.

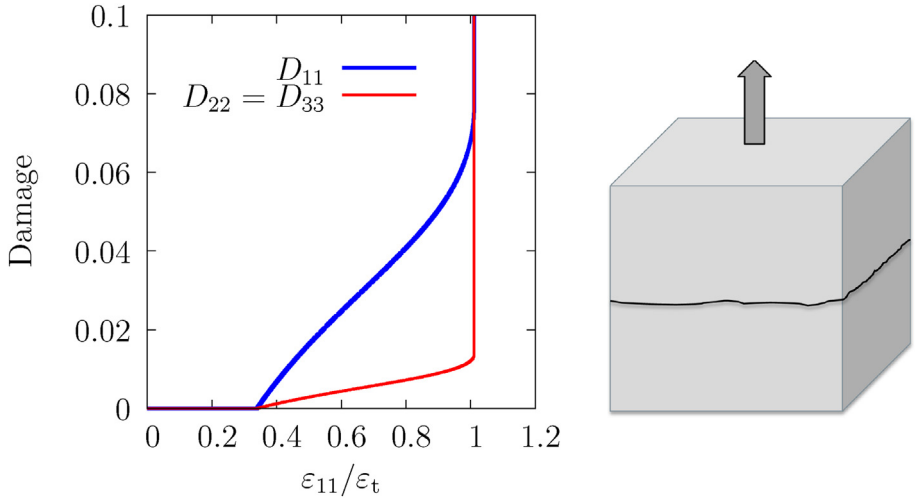

Fig. 6. Damage-strain behaviour in unconfined uniaxial tension. Figure on the RHS illustrates the tensile failure mode.

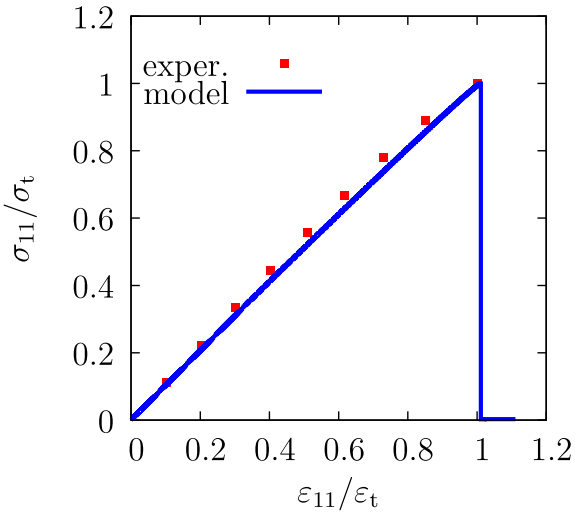

Fig. 7. Stress–strain behaviour in unconfined uniaxial tension.

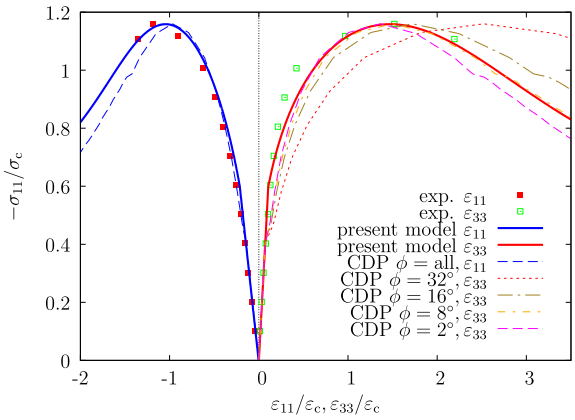

Fig. 8. Stress–strain behaviour in equibiaxial compression with experimental results from Kupfer et al. (1969). The Abaqus CDP model responses are shown for four values of the dilatation angle. Notice that different dilatation angle gives the best fit to experimental data in comparison to unconfined uniaxial compression (see Fig. 4) for the CDP model.

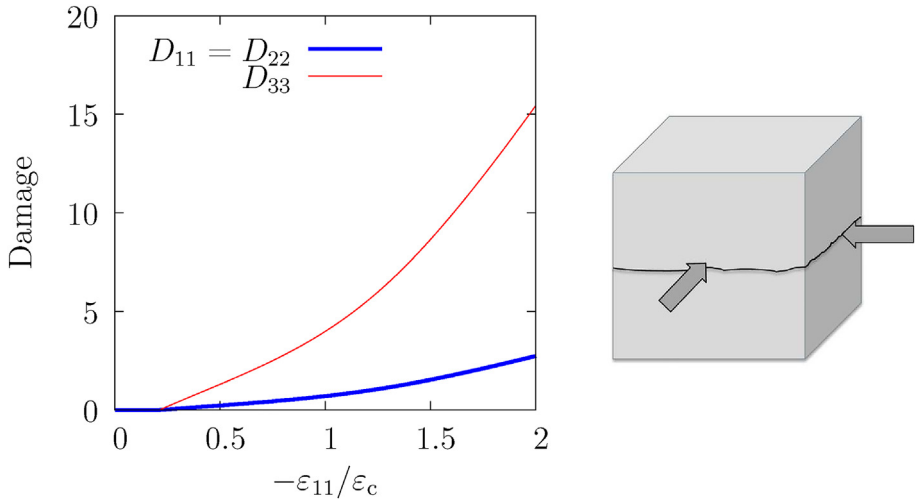

Fig. 9. Damage-strain behaviour in equibiaxial compression ($\sigma_{11} = \sigma_{22}$). Damage is the largest in the 33-direction, i.e. the fracture mode corresponds splitting along the compressive plane illustrated in the figure on the RHS.

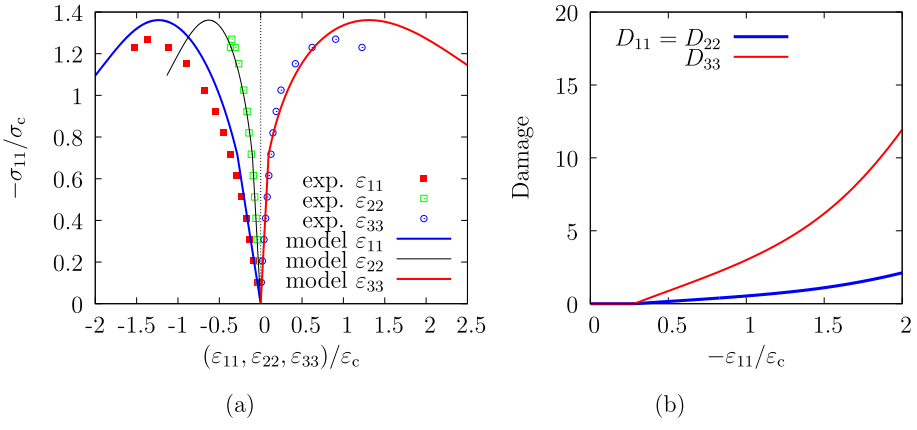

Fig. 10. (a) Stress–strain behaviour in biaxial compression for stress ratio $\sigma_{11}/\sigma_{22} = -1/-0.52$ with experimental results from Kupfer et al. (1969) and (b) damage-strain behaviour.

ize the problem would be to include strain-rate effects or spatial gradients into the model. An early attempt to cope with this problem is also provided by Askes et al. (2021) where a simple scalar damage model is regularized by adding second gradient of damage to the dissipation potential, see also Hillerborg et al. (1976), Markeset and Hillerborg (1995), Fremond et al. (1996), Santaoja (2004). In the case of second order damage tensor, there are more options how the gradient terms can be included into the model.

Further improvements would be the inclusion of irreversible strains in the model to handle cyclic loadings. Inelasticity in quasi-brittle materials is closely related to damage, i.e. frictional sliding along the cracked surfaces.

6. Concluding remarks

In this paper, a thermodynamically consistent formulation to model anisotropic damage for quasi-brittle materials is proposed. The model is based on proper expressions for the specific Gibbs free energy and the complementary form of the dissipation potential. Damaging of the material is described by a symmetric positive definite second order damage tensor. In this formulation the values of the components in the damage tensor do not have an upper bound, thus facilitating a continuous numerical implementation. Especially, the failure surface is formulated in such a way that it will mimic the behaviour of the well known Ottosen's four parameter failure surface. The formulation is basically non-associated, however, the formulation follows closely the one for the standard dissipative solid.

One salient feature of the proposed model is its ability to model the failure modes correctly. In uniaxial compression, the mode of failure is axial splitting, i.e. the damaged zones are aligned parallel to the direction of the compressive stress. In tension, the failure takes place in a plane perpendicular to the applied stress. The obtained results compare favourably with the well-known experimental results found in literature.

CRediT authorship contribution statement

Jani Vilppo: Conceptualization, Methodology, Software, Validation, Writing - review & editing. **Reijo Kouhia:** Conceptualization, Methodology, Writing - original draft, Supervision, Funding acquisition. **Juha Hartikainen:** Conceptualization, Methodology, Writing - review & editing. **Kari Kolari:** Conceptualization, Methodology, Writing - review & editing. **Alexis Fedoroff:** Writing - review & editing. **Kim Calonius:** Writing - review & editing, Funding acquisition.

Declaration of Competing Interest

The authors declare that they have no known competing financial interests or personal relationships that could have appeared to influence the work reported in this paper.

Acknowledgements

This work was partially funded by the CONFIT project which belongs into SAFIR2022, The Finnish Research Programme on Nuclear Power Plant Safety 2019–2022. Main funding organisations of SAFIR2022 are the Finnish State Nuclear Waste Management Fund (VYR) and VTT Technical Research Center of Finland Ltd.

Jani Vilppo wants also to thank the Auramo-foundation and the Concrete Association of Finland (BY) for financial support.

Appendix A

In order to solve the constitutive equations, implicit Euler method together with Newton–Raphson itarative technique has been applied. The solution algorithm is summarized as follows.

1. Increase strain the incremental value $\Delta\boldsymbol{\varepsilon}$and compute the trial elastic stress

$$\boldsymbol{\varepsilon}_{n+1} = \boldsymbol{\varepsilon}_n + \Delta\boldsymbol{\varepsilon}, \tag{78}$$

$$\boldsymbol{\sigma}^{\text{trial}}_{n+1} = \boldsymbol{C}(\boldsymbol{D}_n)(\boldsymbol{\varepsilon}_n + \Delta\boldsymbol{\varepsilon}) = \boldsymbol{\sigma}_n + \boldsymbol{C}(\boldsymbol{D}_n)\Delta\boldsymbol{\varepsilon}, \tag{79}$$

$$\boldsymbol{Y}^{\text{trial}}_{n+1} = \frac{1}{4G}(\boldsymbol{s}^{\text{trial}}_{n+1})^2 + \frac{\chi}{18K_{\text{b}}}(\text{tr}\boldsymbol{\sigma}^{\text{trial}}_{n+1})^2\boldsymbol{I}, \tag{80}$$

where the subscripts correspond to the step numbers and the elasticity tensor $\boldsymbol{C}(\boldsymbol{D})$ is the inverse of the compliance tensor $\boldsymbol{L}(\boldsymbol{D})$.

2. Check the damage condition

$$f^{\text{trial}}_{n+1} = \frac{AJ_2}{\sigma_{\text{c0}}} + \Lambda\sqrt{J_2} + BI_1 - (\sigma_{\text{c0}} + K(\kappa_n)), \tag{81}$$

where $J_2 = \frac{1}{2}\text{tr}((\boldsymbol{s}^{\text{trial}}_{n+1})^2)$and $I_1 = \text{tr}(\boldsymbol{\sigma}^{\text{trial}}_{n+1})$.
IF $f^{\text{trial}}_{n+1} \leqslant 0$ THEN:
Set $\boldsymbol{\varepsilon}_n = \boldsymbol{\varepsilon}_{n+1}$ & EXIT.
ENDIF.

3. Solve $f(\lambda_{n+1}) = 0$.
Use Newton–Raphson iterative method.

- Compute the iterative change $\delta\lambda$

$$f(\lambda^i_{n+1}) + f'(\lambda^i_{n+1})\delta\lambda = 0. \tag{82}$$

$$f(\lambda^i_{n+1}) = f(\boldsymbol{Y}^i_{n+1}, K^i_{n+1}; \boldsymbol{\sigma}^i_{n+1}). \tag{83}$$

$$\delta\lambda = \lambda^{i+1}_{n+1} - \lambda^i_{n+1} \tag{84}$$

where the superscripts refer to iteration number.

- Update $\boldsymbol{D}$

$$\boldsymbol{D}^{i+1}_{n+1} = \boldsymbol{D}^i_{n+1} + \delta\lambda\frac{\partial f^i_{n+1}}{\partial \boldsymbol{Y}^i_{n+1}}. \tag{85}$$

- Update K

$$\kappa^{i+1}_{n+1} = \kappa^i_{n+1} + \delta\lambda, \tag{86}$$

$$K^{i+1}_{n+1} = \frac{H_0\kappa^{i+1}_{n+1}}{\kappa_0^2}(1 - \frac{\kappa^{i+1}_{n+1}}{\kappa_0}) \tag{87}$$

.

- Update $\boldsymbol{\sigma}$

$$\boldsymbol{\sigma}^{i+1}_{n+1} = \boldsymbol{C}^{i+1}_{n+1}(\boldsymbol{D}^{i+1}_{n+1})\boldsymbol{\varepsilon}_{n+1}. \tag{88}$$

References

Adams, M., Sines, G., 1978. Crack extension from flaws in a brittle material subjected to compression. Tectonophysics 49, 97–118.

Askes, H., Hartikainen, J., Kolari, K., Kouhia, R., Saksala, T., Vilppo, J., 2021. An investigation into the behaviour of the Kachanov-Rabotnov type continuum damage model. Accepted for presentation in the XXV ICTAM Congress, 2021, Milano, Italy..

Badel, P., Godard, V., Leblond, J.B., 2007. Application of some anisotropic damage model to the prediction of the failure of some complex industrial concrete structure. Int. J. Solids Struct. 44, 5848–5874.

Balmer, G., 1949. Shearing strength of concrete under high triaxial stress–Computation of Mohr's envelope as a curve. Technical Report SP-23. Bureau of Reclamation, Department of the Interior, Stuctural Research Laboratory.

Basista, M., 2003. Micromechanics of damage in brittle solids. In: Skrzypek, J., Ganczarski, A. (Eds.), Anisotropic Behaviour of Damaged Materials volume 9 of Lecture Notes in Applied and Computational Mechanics. Springer-Verlag, pp. 221–258.

Baant, Z., Oh, B., 1985. Microplane model for progressive fcature of concrete and rock. J. Eng. Mech. ASCE 111, 559–582..
Bažant, Z.P., Caner, F.C., Carol, I., Adley, M.D., Akers, S.A., 2000. Microplane model M4 for concrete. I: formulation with work-conjugate deviatoric stress. J. Eng. Mech. 126, 944–953.
Benkemoun, N., Hautefeuille, M., Colliat, J.B., Ibrahimbegovic, A., 2010. Failure of heterogeneous materials: 3d meso-scale fe models with embedded discontinuities. Int. J. Numer. Methods Eng. 82, 1671–1688.
Brace, W., Bombolakis, E., 1963. A note on brittle crack growth in compression. J. Geophys. Res. 68, 3709–3713.
Bresler, B., Pister, K., 1958. Strength of concrete under combined stresses. Proc. ACI J., 321–345
Cauvin, A., Testa, R.B., 1999. Damage mechanics: basic variables in continuum theories. Int. J. Solids Struct. 36, 747–761.
Červenka, J., Papanikolaou, V.K., 2008. Three dimensional combined fracture? Plastic material model for concrete. Int. J. Plast. 24, 2192–2220.
Chaboche, J.L., 1993. Development of continuum damage mechanics for elastic solids sustaining anisotropic and unilateral damage. Int. J. Damage Mech. 2, 311–329.
Cicekli, U., Voyiadjis, G., Al-Rub, R.A., 2007. A plasticity and anisotropic damage model for plain concrete. Int. J. Plast. 23, 1874–1900.
Contrafatto, L., Cuomo, M., 2002. A new thermodynamically consistent continuum model for hardening plasticity coupled with damage. Int. J. Solids Struct. 39, 6241–6271.
Contrafatto, L., Cuomo, M., 2003. Elastic-plastic damaging behaviour of concrete: a generalized Ottosen criterion. In: Onate, E., Owen, D. (Eds.), VII International Conference of Computational Plasticity COMPLAS 2003. CIMNE, Barcelona.
Contrafatto, L., Cuomo, M., 2006. A framework of elastic? Plastic damaging model for concrete under multiaxial stress states. Int. J. Plast. 22, 2272–2300.
Contrafatto, L., Cuomo, M., 2007. Comparison of two forms of strain decomposition in an elastic-plastic damaging model for concrete. Model. Simul. Mater. Sci. Eng. 15, S405–S423.
Dahl, K., 1992. A failure criterion for normal and high strength concrete. Technical Report 286. Department of Structural Engineering, Technical University of Denmark..
Dassault Systémes, 2020. Abaqus unified FEA. Simulia..
Davison, L., Stevens, A., 1973. Thermodynamical constitution of spalling elastic bodies. J. Appl. Phys. 44, 668–674.
Dragon, A., Halm, D., Désoyer, T., 2000. Anisotropic damage in quasi-brittle solids: modelling, computational issues and applications. Comput. Methods Appl. Mech. Eng. 183, 331–352.
Dragon, A., Mróz, Z., 1979. A continuum model for plastic-brittle behavior of rock and concrete. Int. J. Eng. Sci. 17, 121–137.
Etse, G., Willam, K., 1994. Fracture energy formulation for inelastic behavior of plain concrete. J. Eng. Mech., ASCE 120, 1983–2011.
Frémond, M., 2002. Non-Smooth Thermomechanics. Springer, Berlin.
Frémond, M., Nedjar, B., 1996. Damage, gradient of damage and principle of virtual power. Int. J. Solids Struct. 33, 1083–1103.
Gálvez, J., Červenka, J., Cendón, D., Saouma, V., 2002. A discrete crack approach to normal/shear cracking of concrete. Cem. Concr. Res. 32, 1567–1585.
Grassl, P., Jirásek, M., 2006. Damage-plastic model for concrete failure. Int. J. Solids Struct. 43, 7166–7196.
Grassl, P., Lundgren, K., Gylltoft, K., 2002. Concrete in compression, a plasticity theory with a novel hardening law. Int. J. Solids Struct. 39, 5205–5223.
Grassl, P., Xenos, D., Nyström, U., Rempling, R., Gylltoft, K., 2013. CDPM2: a damage-plasticity approach to modelling te failure of concrete. Int. J. Solids Struct. 50, 3805–3816.
Halm, D., Dragon, A., Charles, Y., 2003. Damage model for quasi-brittle solids: coupled effects of induced and initial anisotropy. J. Phys. IV France 105, 313–320.
Hillerborg, A., Modéer, M., Petersson, P.E., 1976. Analysis of crack formation and crack growth in concrete by means of fracture mechanics and finite elements. Cem. Concr. Res. 6, 773–781.
Horii, H., Nemat-Nasser, S., 1982. Compression induced nonplanar crack extension with application to splitting, exfoliation, and rockburst. J. Geophys. Res. 87, 6805–6821.
Hsieh, S., Ting, E., Chen, W., 1979. An elastic-fracture model for concrete, in: Proceedings of the third Eng. Mech. Div. Spec. Concf. ASCE, Austin, pp. 437–440..
Ibrahimbegović, A., Marcovic, D., Gatuingt, F., 2003. Constitutive model of coupled damage-plasticity and its finite element implementation. Revue Européenne des Eléments Finis 12, 381–405.
Jason, L., Huerta, A., Pijaudier-Cabot, G., Ghavamian, S., 2006. An elastic plastic damage formulation for concrete: application to elementary tests and comparison with an anisotropic damage model. Comput. Methods Appl. Mech. Eng. 195, 7077–7092.
Jefferson, A., 2003. Craft–a plastic-damage-contact model for concrete. i. Model theory and thermodynamic considerations. Int. J. Solids Struct. 40, 5973–5999.
Jefferson, A., Mihai, I., Tenchev, R., Alnaas, W., Cole, G., Lyons, P., 2016. A plastic-damage-contact constitutive model for concrete with smoothed evolution functions. Comput. Struct. 169, 40–56.
Ju, J.W., 1990. Isotropic and anisotropic damage variables in continuum damage mechanics. J. Eng. Mech. 116, 2764–2770.
Kachanov, L., 1958. On the creep fracture time. Iz. An SSSR Ofd. Techn. Nauk., 26–31 (in Russian)
Kachanov, M., 1992. Effective elastic properties of cracked solids: critical review of some basic concepts. Appl. Mech. Rev. 45, 304–335.
Kendall, K., 1978. Complexities of compression fracture. Proc. Roy. Soc. A 361, 245–263.
Kolari, K., 2007. Damage mechanics model for brittle failure of transversely isotropic solids – finite element implementation. Technical Report 628. VTT Publications. Espoo..
Kolari, K., 2017. A complete three-dimensional continuum model of wing-crack growth in granular brittle solids. Int. J. Solids Struct. 115–116, 27–42.
Kupfer, H., Hilsdorf, H., Rüsch, H., 1969. Behaviour of concrete under biaxial stresses. J. Am. Concr. Inst. 66, 656–666.
Lee, J., 1996. Theory and implementation of plastic-damage model for concrete structures under cyclic and dynamic loading. Ph.D. thesis. University of California, Berkeley..
Lee, J., Fenves, G., 1998. Plastic-damage model for cyclic loading of concrete structures. J. Eng. Mech., ASCE 124, 892–900.
Lu, D., Du, X., Wang, G., Zhou, A., Li, A., 2016. A three-dimensional elastoplastic constitutive model for concrete. Comput. Struct. 163, 41–55.
Lu, D., Zhou, X., Du, X., Wang, G., 2019. A 3d fractional elastoplastic constitutive model for concrete material. Int. J. Solids Struct. 165, 160–175.
Lu, D., Zhou, X., Du, X., Wang, G., 2020. 3d dynamic elastoplastic constitutive model of concrete within the framework of rate-dependent consistency condition. J. Eng. Mech. 146, 04020124.
Lubarda, V., Krajcinovic, D., Mastilovic, S., 1994. Damage model for brittle elastic solids with unequal tensile and compressive strengths. Eng. Fract. Mech. 49, 681–697.
Lubliner, J., Oliver, J., Oller, S., Oñate, E., 1989. A plastic-damage model for concrete. Int. J. Solids Struct. 25, 299–326.
Markeset, G., Hillerborg, A., 1995. Softening of concrete in compression – localization and size effects. Cem. Concr. Res. 25, 702–708.
Mazars, J., Pijaudier-Cabot, G., 1989. Continuum damage theory – application to concrete. J. Eng. Mech., ASCE 115, 345–365.
Mazars, J., Pijaudier-Cabot, G., 1996. From damage to fracture mechanics and conversely: a combined approach. Int. J. Solids Struct. 33, 3327–3342.
Menétrey, P., Willam, K., 1995. A triaxial failure criterion for concrete and its generalization. ACI Struct. J. 92, 311–318.
Mikkola, M., Piila, P., 1984. Nonlinear response of concrete by use of the damage theory. In: Proceedings of the International Conference on Computer-Aided Analysis and design of Concrete Structures. Pineridge Press, Swansea, pp. 179–189.
Mikkola, M., Schnobrich, W.C., 1970. Material behavior characteristics for reinforced concrete shells stressed beyond the elastic range. Technical Report 367. University of Illinois, Urbana-Champaign..
Mondal, S., Olsen-Kettle, L., Gross, L., 2019. Simulating damage evolution and fracture propagation in sandstone containing a preexisting 3-d surface flaw under uniaxial compression. Int. J. Numer. Anal. Meth. Geomech. 43, 1448–1466. https://onlinelibrary.wiley.com/doi/pdf/10.1002/nag.2908.
Murakami, S., 2012. Continuum Damage Mechanics. Volume 185 of Solid Mechanics and Its Applications. Springer, Netherlands..
Murakami, S., Kamiya, K., 1997. Constitutive and damage evolution equations of elastic-brittle materials based on irreversible thermodynamics. Int. J. Mech. Sci. 39, 473–486.
Murakami, S., Ohno, N., 1981. A continuum theory of creep damage. In: The 3rd IUTAM Symposium on Creep in Structures, pp. 422–444.
Nguyen, G., Korsunsky, A., 2008. Development of an approach to constitutive modelling of concrete: isotropic damage coupled with plasticity. Int. J. Solids Struct. 45, 5483–5501.
Oliveira, D., Penna, S., Pitangueira, R., 2020. Elastoplastic constitutive modeling for concrete: a theoretical and computatioal approach. IBRACON Struct. Mater. J. 13, 171–182.
Olsen-Kettle, L., 2018. Quantifying the orthotropic damage tensor for composites undergoing damage-induced anisotropy using ultrasonic investigations. Compos. Struct. 204, 701–711.
Olsen-Kettle, L., 2018. Using ultrasonic investigations to develop anisotropic damage models for initially transverse isotropic materials undergoing damage to remain transverse isotropic. Int. J. Solids Struct. 138, 155–165.
Ortiz, M., 1985. A constitutive theory for the ielastic behavior of concrete. Mech. Mater. 4, 67–93.
Ottosen, N., 1977. A failure criterion for concrete. J. Eng. Mech., ASCE 103, 527–535.
Ottosen, N., 1980. Nonlinear Finite Element Analysis of Concrete Structures. Technical Report Risø-R-411. RisøNational Laboratory. DK-4000 Roskilde, Denmark.
Ottosen, N., Ristinmaa, M., 2005. The Mechanics of Constitutive Modeling. Elsevier.
Papanikolaou, V., Kappos, A., 2007. Confinement-sensiive plasticity constitutive model for concrete in triaxial compression. Int. J. Solids Struct. 44, 7021–7048.
Richart, F., Braendtzaeg, A., Brown, R., 1928. A study of the failure of concrete under combined compressive stresses. Bulletin No. 185, University of Illinois, Engineering Experiment Station, Urbana, IL..
Rimkus, A., Cervenka, V., Gribniak, V., Cervenka, J., 2020. Uncertainty of the smeared crack model applied to rc beams. Eng. Fract. Mech. 233, 107088.
Santaoja, K., 2004. Gradient theory from the thermomechanics point of view. Eng. Fract. Mech. 71, 557–566.
Schreyer, H.L., 2007. Modelling surface orientation and stress at failure of concrete and geological materials. Int. J. Numer. Anal. Meth. Geomech. 31, 147–171. nag.2347.
Simo, J., Ju, J., 1987. Strain- and stress based continuum damage models-i. formulation. Int. J. Solids Struct. 23, 821–840.

Tahaei Yaghoubi, S., Kouhia, R., Hartikainen, J., Kolari, K., 2014. A continuum damage model based on Ottosen's four parameter failure criterion for concrete. J. Struct. Mech. (Rakenteiden Mekaniikka) 47, 50–66.
Valentini, B., Hofstetter, G., 2013. Review and enhancement of 3d concrete models for large-scale numerical simulations of concrete structures. Int. J. Numer. Anal. Meth. Geomech. 37, 221–246.
van Mier, J., 1986. Fracture of concrete under complex stress. Heron 31, 1–90.
Voyiadjis, G., Taqieddin, Z., 2009. Elastic plastic and damage model for concrete materials: Part i-theoretical formulation. Int. J. Struct. Changes Solids-Mech. Appl. 1, 31–59.
Voyiadjis, G., Taqieddin, Z., Kattan, P., 2008. Anisotropic damage-plasticity model for concrete. Int. J. Plast. 24, 1946–1965.
Willam, K., Warnke, E., 1975. Constitutive model for the triaxial behaviour of concrete. In: IABSE Proceedings, Seminar on Concrete Structures Subjected to Triaxial Stresses, Bergamo, Italy May 17–19, 1974, pp. 1–30..
Yazdani, S., Schreyer, H., 1988. An anisotropic damage model with dilatation for concrete. Mech. Mater. 7, 231–244.
Yazdani, S., Schreyer, H., 1990. Combined plasticity and damage mechanics model for plain concrete. J. Eng. Mech., ASCE 116, 1435–1450.
Zhang, X., Wu, H., Li, J., Pi, A., Huang, F., 2020. A constitutive model of concrete based on Ottosen yield criterion. Int. J. Solids Struct. 193–194, 79–89.